Title

Anionic Sublattices in Halide Solid Electrolytes: A Case Study with High-Pressure Phase of Li3ScCl6

Authors

Ding, Fenghua

Doi, Atsunori

Ogawa, Takafumi

et al.

Publication Date

2024-02-16

DOI

10.1002/anie.202401779

Pressure-Induced Anionic Sublattice Change in the Solid Electrolyte Li_3ScCl_6 with Enhanced Electrochemical Stability

Fenghua Ding,[†] Atsunori Doi,[‡] Takafumi Ogawa,[§] Hiroki Ubukata,[†] Tong Zhu,[†] Daichi Kato,[†] Cédric Tassel,[†] Itaru Oikawa,[¶] Naoki Inui,[†‡] Satoru Kuze,[†‡] Tsutomu Yamabayashi,[Φ‡] Kotaro Fujii,[∥] Masatomo Yashima,[∥] Xing Ou,[ζ] Zhijian Wang,[ζ] Xiaobo Min,[ζ] Koji Fujita,[†] Hitoshi Takamura,[¶] Akihide Kuwabara,[§] Kent J. Griffith,[£] Zhang Lin,[ζ] Liyuan Chai,[ζ] and Hiroshi Kageyama[†,*]

[†]Graduate School of Engineering, Kyoto University, Kyoto 615-8510, Japan

[‡]Advanced Materials Development Laboratory, Sumitomo Chemical Co. Ltd., Tsukuba 300-3294, Japan

[§]Nanostructures Research Laboratory, Japan Fine Ceramics Center, Nagoya 456-8587, Japan

[¶]Department of Materials Science, Graduate School of Engineering, Tohoku University, Sendai 980-8579, Japan

[Φ]Energy & Functional Materials Research Laboratory, Sumitomo Chemical Co. Ltd., Niihama 792-8521, Japan

[∥] Department of Chemistry, School of Science, Tokyo Institute of Technology, 2-12-1-W4-17, O-okayama, Meguro-ku, Tokyo 152-8551, Japan

[ζ]School of Metallurgy and Environment, Central South University, Changsha, 410083, PR China

[£]Department of Chemistry & Biochemistry, University of California, San Diego, La Jolla, California 92093, USA

ABSTRACT: The manipulation of sublattices in crystal structures holds significant importance and broad interest due to its potential for designing innovative structures and fine-tuning functional materials. For example, both experimental and theoretical studies indicate that there is a ~~connected~~ relationship between anion packing and ionic transport in lithium solid electrolytes. However, achieving precise control over the anionic sublattice remains a challenging task that requires a deeper understanding of ~~the~~ fundamental crystal chemistry~~s~~. In this study, we present a high-pressure polymorph of Li_3ScCl_6 (denoted as γ-Li_3ScCl_6)~~,~~ as a lithium solid electrolyte. The structure and function of this material are characterized using a combination of diffraction techniques (single-crystal and synchrotron), spectroscopy (impedance, X-ray photoelectron yield~~ spectroscopy~~, and NMR), and ab initio calculations. Under a pressure of 5 GPa, γ-Li_3ScCl_6 is synthesized and crystallizes into a hexagonal polar and chiral space group, $P6_3mc$, which is maintained at ambient pressure. The formation of a hexagonal close-packed (hcp) anion lattice is attributed to an increase in the cation--anion radius ratio induced by pressure. The ionic conductivity of γ-Li_3ScCl_6 at room temperature is measured to be 0.21 mS/cm. Electrochemical tests on symmetric cells demonstrate the improved electrochemical stability of γ-Li_3ScCl_6 against a Li-In anode. Furthermore, an all-solid-state lithium battery (ASSLB) ~~configuration~~ of Li-In/γ-Li_3ScCl_6/NCM111 exhibits a reversible capacity of 116 mAh/g without the need for a sulfide electrolyte intermediate protection layer on the anode or applied passivating coatings on the cathode. These findings open up new avenues and design principles for lithium SSEs, enabling routes for the materials exploration ~~of novel exceptional materials~~ and the enhancement of ~~their~~ electrochemical properties.

Introduction

All-solid-state lithium-ion batteries have gained significant interest due to their ~~potential~~ prospect for achieving high energy density and addressing safety concerns associated with lithium-ion batteries that use flammable nonaqueous electrolytes.[1,2] The development of solid-state electrolytes (SSEs) plays a crucial role in the advancement of ASSLBs. Though many sulfide-based SSEs (e.g., $Li_{10}GeP_2S_{12}$ and $Li_7P_2S_8I$)[3,4] exhibit high ionic conductivities, their limited electrochemical oxidation stability renders them incompatible with conventional cathode materials, such as $LiCoO_2$ and $Li(Ni_{1-x-y}Mn_xCo_yO_2)$.[5–8] On the other hand, oxide-based SSEs generally offer better high-voltage oxidation stability, but their production requires a high-temperature sintering process and they possess rigid mechanical properties, which can impede commercial scalability.[9,10]

The oxidation potential of anions is the key factor in determining the electrochemical stability of SSE at high voltages, with the order ~~of~~ being $N^{3-} < P^{3-} < H^- << S^{2-} < O^{2-} < Br^- < Cl^- << F^-$.[11–13] In this regard, halide SSEs, especially chloride-based SSEs, are of particular ~~importance~~ promise for use in ASSLBs.[13–16] There have been a few examples of chloride SSEs that exhibit high ionic conductivity, such as monoclinic Li_3ScCl_6 (denoted as α-Li_3ScCl_6 afterward), Li_3InCl_6, and Li_3YCl_6.[5–7,14] By employing ~~them~~ these chlorides as SSEs, 4 V ceramic all-solid-state Li-ion batteries were realized with high coulombic efficiencies without extra coatings on the cathode active material.[6,7,17] The high oxidation potentials of the chloride SSEs are theoretically demonstrated,[18,19] but still not sufficient for lithium metal, and, in fact, these chlorides show~~ed~~ electrochemical instability when in contact with ~~the~~ a Li anode.[5–7,14] As a result, a layer of sulfide electrolyte, *e.g.*, $Li_{6.7}Si_{0.7}Sb_{0.3}S_5I$, is needed between the Li_3MCl_6 SSE and the Li anode,[7,8,20] or an indium anode is used merely for demonstration.[5,6] Only α-Li_3ScCl_6[6] and $Li_{0.388}Ta_{0.238}La_{0.475}Cl_3$[21] have been documented to cycle directly against the Li anode, despite the former experiencing significant voltage polarization.

In general, the anion lattice is one of the most critical metrics for ionic conductor design.[13,22] To achieve high ionic conductivities, the body-centered cubic (bcc) anion lattice is often favored over the cubic close-packed (ccp) and hexagonal close-packed (hcp) lattices~~, to achieve high ionic conductivities~~. This is attributed to the bcc anion lattice providing low activation barriers and high ionic conductivity by allowing Li^+ hops between adjacent tetrahedral sites (denoted as T–T path).[22] Although this fundamental guideline emerges predominantly from studies on sulfide-based electrolytes, showcased by examples like $Li_{10}GeP_2S_{12}$[3] and $Li_7P_3S_{11}$,[23] it is believed to hold true across other pairings of mobile cations and immobile anion lattices.[22] Yet, in the realm of ~~chloride~~ halide SSEs, no bcc anion lattice has been identified. Theoretical studies identified ccp and hcp lattices for the reported compounds, e.g., Li_3YBr_6 (ccp) and Li_3YCl_6 (hcp).[5,20,24] In the ccp lattice, Li^+ ionic diffusion occurs through a three-dimensional network, where Li^+ ions hop to the other octahedral sites through tetrahedral sites (denoted as O–T–O path). In an hcp lattice, Li^+ conductivity proceeds via anisotropic one-dimensional channels, in which Li ions hop among face-sharing octahedral sites through existing vacant sites (denoted as O–O path).[13] Within these anion lattice categories, aliovalent substitution of metal ions has been widely used to tune the vacancies on cation sites and improve the ionic conductivity of chloride SSEs, *e.g.*, $Li_{3-x}M_{1-x}Zr_xCl_6$ (M = Y, Er).[7] Moreover, different kinetically stabilized phases have been reported to possess different cation/vacancy arrangements. For example, β-Li_3YCl_6 with its hcp anion lattice exists metastably below 600 K *versus* α-Li_3YCl_6 that is stable above 600 K.[25] ~~And a~~ In another case, a spinel-type metastable phase of $Li_2Sc_{2/3}Cl_4$ with the ccp anion lattice emerg~~ed when subjected to a longer reaction time of 48 hours, as opposed to~~ from α-Li_3ScCl_6 when the reaction time is increased from 12 to 48 hours~~which was formed after 12 hours at 650 °C~~.[8] While these SSEs achieved high ionic conductivities, the electrochemical reduction instability issues with the Li anode remain unresolved.

To address this issue, two guiding principles could be referenced[11,19]: (a) fostering stronger chemical bonds between cations and anions to reduce the propensity for reduction reactions in the electrolytes, and (b) preventing the formation of electronic conductors in the reduction products. On the basis of these concepts, we selected the Li-Sc-Cl system, particularly as α-Li_3ScCl_6 stands out as the pioneering chloride-SSE known to cycle directly against ~~the~~ Li metal.[6] By adopting high-pressure synthesis techniques, it is anticipated that denser configurations and increased electron density overlap between neighboring atoms will emerge, resulting in reinforced chemical bonds.[26] In this context, we present the synthesis and characterization of a novel polymorph of Li_3ScCl_6 (denoted as γ-Li_3ScCl_6), achieved using high pressure. The anionic sublattices among the polymorphs of Li_3ScCl_6 are comprehensively compared. We also demonstrate that Li-In/γ-Li_3ScCl_6/NCM111 ASSLB exhibits a high reversible capacity of 116 mAh/g and good cyclability performance without either a sulfide electrolyte protection layer against the Li-In anode or extra coatings on the ~~cathode~~ NCM111 cathode.

Experimental procedures

Synthesis. To prepare γ-Li_3ScCl_6, stoichiometric LiCl (Alfa Aesar, 99.9%) and $ScCl_3$ (Sigma-Aldrich, 99.9%) were mixed in a glove box with an N_2 atmosphere. The mixture was then pressed into a pellet with gold foil as protection. The pellet was placed into a hand-made gold crucible and inserted into a boron nitride (BN) sleeve with BN caps. Next, the assembly was inserted into a graphite tube and enclosed in a pyrophyllite cube for a high-pressure reaction. The sample cell was pressed to 5 GPa in 1 hour and then heated to 1000 °C within 15 min. After holding for 3 hours at this temperature, the samples were quenched to room temperature within 5

min before the pressure was released to ambient pressure in 2 hours. For single crystals growth, a slower cooling rate of 70 °C/h was applied. The reported α-Li_3ScCl_6 was prepared by heating a stoichiometric mixture of LiCl and $ScCl_3$ at 650 °C for 12 hours in a sealed silica tube according to the published procedures.[6]

Structure Solution and Refinement Methods. Colorless, transparent platy crystals were chosen for structure determination. Single-crystal XRD data were collected at 123 K, using a Bruker Kappa APEX 2 CCD diffractometer with monochromated Mo K_α radiation (λ = 0.7107 Å). The crystal-to-detector distance was set to 50 mm. The SAINT program was used for data reduction and integration.[1] The structures were established by direct methods and refined through full-matrix least-squares fitting on F^2 using OLEX2.[2] Numerical absorption corrections were carried out using the SADABS program for an area detector. The structure was solved using SHEL-XS to determine the atomic coordinates of the cations.[2] A check of possible missing symmetry elements by PLATON found no additional symmetry.[3] The refinements of independent Sc sites were done by using free variables to refine the occupancies, while the occupancy of Li sites was obtained through constrained refinement by considering the charge balance.

Powder Synchrotron X-ray Diffraction (SXRD). SXRD measurements for α-Li_3ScCl_6 and γ-Li_3ScCl_6 were performed with λ = 0.42 Å radiation at SPring-8 in Japan (BL02B2 beamline). The as-synthesized samples were sealed in borosilicate capillaries for the measurement due to the hygroscopic property of both compounds. GSAS was used for the refinement.

Nuclear Magnetic Resonance (NMR). NMR spectroscopy was carried out by using a JNM-ECZL-600 spectrometer (JEOL RESONANCE Inc.) operating at a magnetic field of 14.1 T. A 2.5 mm CPMAS probe was used with a zirconia sample rotor spun at variable magic-angle spinning (MAS) rates of up to 25 kHz. The Larmor frequency of observed nuclei was 233.25 MHz for ^{7}Li and 145.79 MHz for ^{45}Sc. ^{7}Li-NMR spectra were collected using a π/6 pulse of 0.75 μs and 4 scans were accumulated at a repetition time of 5 s. For ^{45}Sc-NMR spectra, 1.54 μs pulse length corresponding to a π/24 pulse of a solution reference and 4000 scans were accumulated at a repetition time of 1 s. The observed spectra were referenced to a signal of 1 M LiCl aqueous solution at 0 ppm for ^{7}Li and 1 M $Sc(NO_3)_3$ aqueous solution at 0 ppm for ^{45}Sc. Deconvolution of the spectra was carried out using the Dmfit program. **MAS** について書く

Photoelectron Yield Spectroscopy (PYS). PYS experiments were carried out using a Bunko Keiki BIP-KV201 photoemission spectrometer (accuracy = ±0.02 eV) and an extraction voltage of 10 V under vacuum conditions (< 10^{-2} Pa). In an N_2-filled glovebox (~0.0 ppm O_2), powder samples were placed on conductive carbon tape on glass, which was contacted through the aluminum tape and a gold-coated electrode.

UV-Vis. diffuse reflectance spectroscopy. UV–vis diffuse reflectance spectra were collected with a UV-3600 SHIMADZU UV–vis–NIR spectrophotometer over the spectral range of 200 to 1000 nm at room temperature. Barium sulfate, $BaSO_4$, was used as a standard for the baseline correction. The sample was thoroughly mixed with $BaSO_4$, and this mixture was used for UV–vis measurements. Reflectance spectra were converted to absorbance using the Kubelka–Munk equation.

Impedance Spectroscopy. Ionic conductivities of cold-pressed pellets of γ-Li_3ScCl_6 were measured by AC electrochemical impedance spectroscopy (EIS) with a constant voltage of 100 mV in the frequency range of 1 MHz to 0.1 Hz using a SI 1260 Impedance/Gain-phase Analyzer (Solartron). The γ-Li_3ScCl_6 powder was placed into a custom-made Swagelok cell and pressed at around 15 MPa into a 10 mm diameter disk between two stainless steel rods, which served as blocking electrodes for EIS measurements. All cell preparation was conducted in a glove box with an Ar-protected atmosphere. The prepared cells were then sealed in a desiccator for electrochemical measurements outside the glove box in a temperature-controlled furnace. The EIS measurement for each composition was collected at 25, 40, 80, and 100 °C after being held for 90 mins to ensure temperature stabilization.

Cyclic voltammetry (CV) measurement. The relative electrochemical stability was evaluated by CV measurements using TOSCAT-3100 (Toyo system computer automatic tester) with Li/γ-Li_3ScCl_6/γ-Li_3ScCl_6-C in a scan range of –0.2 to 5 V (vs. Li^+/Li^+) at 0.1 mV/s. For the electrolyte layer, 80 mg of γ-Li_3ScCl_6 was used, while for the ~~a~~ composite cathode, a mixture of 10 mg γ-Li_3ScCl_6 and 10 mg acetylene black carbon~~,~~ was used. The CV measurements for α-Li_3ScCl_6 followed the same procedures.

ASSBs measurement. All-solid-state batteries (ASSBs) employing the γ-Li_3ScCl_6 SSE combined with a commercial $LiNi_{1/3}Co_{1/3}Mn_{1/3}CoO_2$ (NMC111) cathode active material and an In-Li anode were assembled in an argon-filled glovebox. To prepare cathode composites, NMC111 and as-prepared γ-Li_3ScCl_6 with a mass ratio of 70:30 was ground in an agate mortar. 100 mg of γ-Li_3ScCl_6 was compressed at about 15 MPa to form a solid-state electrolyte layer. 6-10 mg cathode composites were spread on one side of γ-Li_3ScCl_6 pellets and pressed at about 5 MPa. A gold foil was used as a current collector on the cathode side. Then a piece of indium and lithium foil (60 mg) was put on another side of γ-Li_3ScCl_6 and pressed at around 5 MPa. The home-made model cells were cycled in the voltage range of 2.5–3.7 V (vs. Li^+/Li-In). ASSB measurements with α-Li_3ScCl_6 followed the same procedures.

DFT calculations. All electronic structure calculations were carried out within the DFT framework using the projector augmented wave (PAW) method, as implemented in the VASP code.[27,28] We employed the PBEsol function[29] for as the exchange-correlation functional and the DFT-D3 Van der Waals corrections by Grimme et al.[30] The used energy cutoff for plane-wave expansion was set to 650 eV. For Brillouin zone (BZ) integrations, Γ-centered ***k***-point meshes with spacing less than 0.4 $Å^{-1}$ were used. The convergence criterion for geometry optimization was set to 0.01 eV/Å. Effective ionic radii were calculated based on the Bader charge analysis.[31] Configurations of atoms in the α-and γ-Li_3ScCl_6 crystals were determined as follows: For γ-Li_3ScCl_6, the lowest-energy configuration was chosen from the examination of all possible configurations (38 in total) in the unit cell including 30 atoms, while, for α-Li_3ScCl_6, the lowest-energy one from ten structures with random distribution on the Li partial occupation sites in the 2×1×2 supercell including 80 atoms.

Density maps of Li-atoms of both crystals at finite temperatures were constructed from trajectories of molecular dynamics (MD) simulations within the NVT-ensemble. Here, the cutoff energy of 270 eV and Γ-point BZ sampling were used, in concurrent with switching to PAW potentials with less valence electrons. To avoid correlation between atoms in periodically aligned cells, the simulation box of γ-Li_3ScCl_6 was expanded to the 1×1×2 supercell, including 60 atoms.

Results and Discussion

To facilitate comparison, we will refer to the previously reported monoclinic structure of Li_3ScCl_6 as α-Li_3ScCl_6 (space group: *C*2/*m*),[6] while the structurally related spinel phase of $Li_2Sc_{2/3}Cl_4$ (space group: *Fd*-3*m*)[8] will be denoted as β-Li_3ScCl_6 after adjusting for composition normalization. Synchrotron XRD data for the powder sample of Li_3ScCl_6 synthesized under a pressure of 5 GPa at 1000 °C, which will be referred to as γ-Li_3ScCl_6, is presented in Figure 1a. The XRD data can be indexed using a primitive hexagonal lattice with room temperature lattice parameters of a = 10.919(9) Å and c = 5.975(7) Å, suggesting that γ-Li_3ScCl_6 is isostructural with trigonal Li_3YCl_6 (space group: *P*–3*m*1) with close slightly contracted lattice constants (a = 11.173(6) Å and c = 6.015(7) Å), though it will be shown that γ-Li_3ScCl_6 crystallizes in a different space group.[32] As expected, the high-pressure γ-Li_3ScCl_6 has a smaller (normalized) cell volume of 617 $Å^3$ compared to the ambient-pressure phase of α-Li_3ScCl_6 (636 $Å^3$, Z = 2). In addition, we have successfully grown single crystals of γ-Li_3ScCl_6 under high pressure with a slow cooling rate from 1000 °C to ambient temperature for 10 hours.

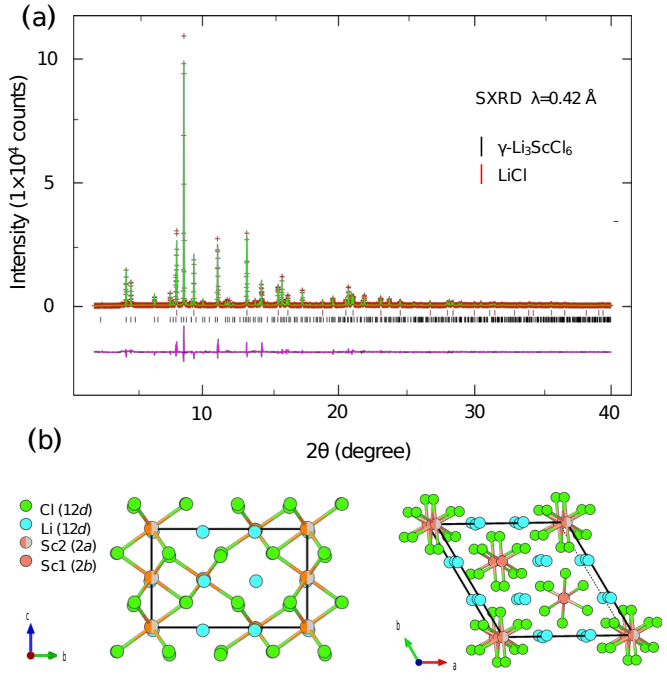

Figure 1. (a) Synchrotron XRD Rietveld refinement of γ-Li_3ScCl_6 at 300 K, using the $P6_3mc$ space group. (b) Ball-and-stick representations of the structure of γ-Li_3ScCl_6 (upperleft) along the *a*-direction and (rightlower) along the *c*-direction. Wyckoff positions and multiplicities are given.

(a)(b)をたてにして、構造をよこに。横長の図が増えると読みにくくなるように思います。

Table S1. Crystal data and structure refinement of γ-Li_3ScCl_6 from single-crystal X-ray diffraction.

Formula weight/g mol^{-1}	278.48
Temperature/K	123
Crystal system	hexagonal
Space group	$P6_3mc$
a/Å	10.831(6)
b/Å	10.831(6)
c/Å	5.924(3)
Volume/Å^3	601.88(7)
Z	3
ρ$_{calc}$/g cm^{-3}	2.305
Crystal size/mm^3	0.03 × 0.03 × 0.02
Radiation	Mo Kα (λ = 0.71073 Å)
2θ range for data	7.524 to 63.514
Index ranges	−16 ≤ h ≤ 12, −10 ≤ k ≤
Reflections collected	3328
Independent reflections	754 [R$_{int}$ = 0.0149, R$_{sigma}$ =
Data/restraints/	754/1/37
Goodness-of-fit on F^2	1.117
Final R indexes [I >= 2σ(I)]	R$_1$ = 0.0212, wR$_2$ = 0.0482
Final R indexes [all data]	R$_1$ = 0.0252, wR$_2$ = 0.0506
Largest diff. peak/hole	0.56/−0.28
Flack parameter	−0.3(2)

The obtained single crystals were also used for structural determination. Remarkably, structural refinement using both powder and single-crystalline samples revealed that γ-Li_3ScCl_6 crystallizes into a polar and chiral space group of $P6_3mc$ (No. 186), not the nonpolar $P\bar{3}m1$ for Li_3YCl_6. The absence of an inversion center was confirmed by second harmonic generation (SHG) measurements on the as-synthesized γ-Li_3ScCl_6 single crystals, which exhibited a non-zero response (Figure S2). Detailed crystallographic parameters can be found in Tables 1 and Table S1. A representative Rietveld refinement of γ-Li_3ScCl_6 (Figure 1a and Table S2) is in good agreement with the refinements obtained from the single-crystal X-ray diffraction analysis (Figure S1). As far as we are aware, this structure represents the first non-centrosymmetric structure among the Li_3MX_6 compounds (where ***M*** ranges from Sc to Y, Sm to Lu, and ***X*** represents F, Cl, and Br). In γ-Li_3ScCl_6, Sc^{3+} in the d^0 electronic state displays a C_3-type distortion with the octahedral center of Sc displaced toward the octahedral face (Figure S3a). This displacement of the octahedral centers, which is ascribed to the second-order Jahn–Teller effect (SOJT) between filled Cl-3p orbitals and empty Sc-3d (t_{2g}) orbitals (Figures S3b-3d), and their uniform alignment along the ***c***-axis give polarization to the entire crystal. Such displacement is almost absent in Li_3YCl_6, which suggests that Sc-Cl in γ-Li_3ScCl_6 is more covalently bonded (vs. Y-Cl in Li_3YCl_6) due to the greater electronegativity of Sc (1.36) compared to Y (1.22).

Table 1. Fractional atomic coordinates and equivalent isotropic displacement parameters (Å^2 × 10^3) for γ-Li_3ScCl_6 at 123 K. U_{eq} is defined as 1/3 of the trace of the orthogonalized U_{ij} tensor. The occupancy of Sc was refined by single-crystal X-ray diffraction analysis, which yielded 0.97 for Sc1 and 0.49 for Sc2, thus fixed to 1 and 1/2, respectively.

Atom	Wyckoff site	Occupancy	*x*	*y*	*z*	*U* (eq)
Li	12*d*	0.75	0.3369(1)	0.3290(1)	0.4700(7)	32(5)
Sc1	2*b*	1	1/3	2/3	0.4875(6)	8.1(2)
Sc2	2*a*	1/2	0	0	0.5068(6)	3.6(4)
Cl1	6*c*	1	0.4424(8)	0.5575(8)	0.7227(3)	10.9(4)
Cl2	6*c*	1	0.2237(8)	0.4475(15)	0.2534(13)	10.2(3)
Cl3	6*c*	1	0.1097(7)	0.2194(14)	0.7552(13)	12.8(3)

γ-Li_3ScCl_6 (Z = 3) has two crystallographically independent sites for Sc^{3+}, one site for Li^+, and three sites for Cl^-. Both cations are octahedrally coordinated, as depicted in Figures 1b and 1c. Sc1 fully occupies the 2*a* site, and Sc2 at the 2*b* site is half occupied (Table 1). Then, charge neutrality requires 3/4 occupancy of Li at the 12*d* site. The bond valence sums (BVS)[33] for Li and Sc1 are calculated to be 0.99 and 3.03, respectively, consistent with their formal valences, whereas Sc2 exhibits a slightly under-bonded value of 2.64, possibly related to its 50% occupancy. The single-site occupation of Li is further supported by the ^{7}Li MAS-NMR spectrum with a sharp peak centered at –0.8 ppm (Figure 2a). On the other hand, the ^{45}Sc MAS-NMR spectrum displays a broad peak of around 235 ppm due to the presence of quadrupole splitting and two (Sc1/Sc2) sites (Figure 2b). We simulated the NMR peak positions using a 1 × 1 × 2 supercell taking into account the partial occupancies of Li and Sc2 (Figure S4), which provided –0.98 ~ –1.7 ppm for Li and 236-238 ppm for Sc, in good agreement with the experimental observation.

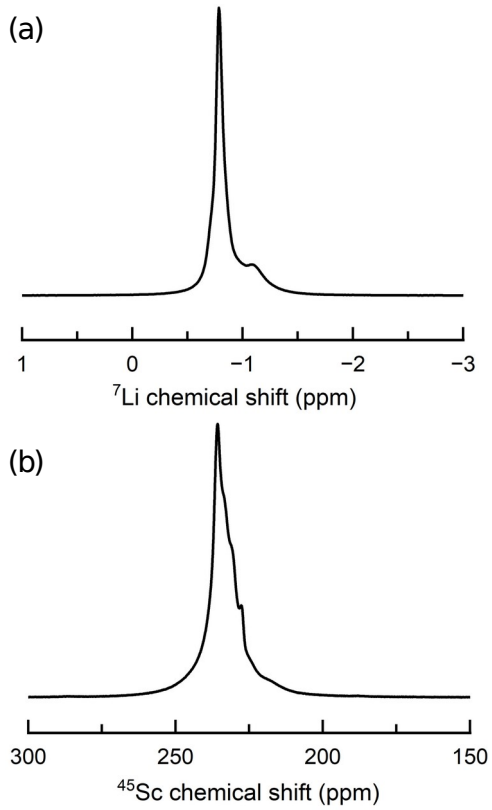

Figure 2. (a) ^{7}Li-NMR and (b) ^{45}Sc-NMR spectra for γ-Li_3ScCl_6. The MAS rate was 25 kHz. A minor shoulder observed at –1.1 ppm in (a) is attributed to LiCl, as confirmed by XRD measurements. The details of DFT-assisted simulations are shown in Figure S4.

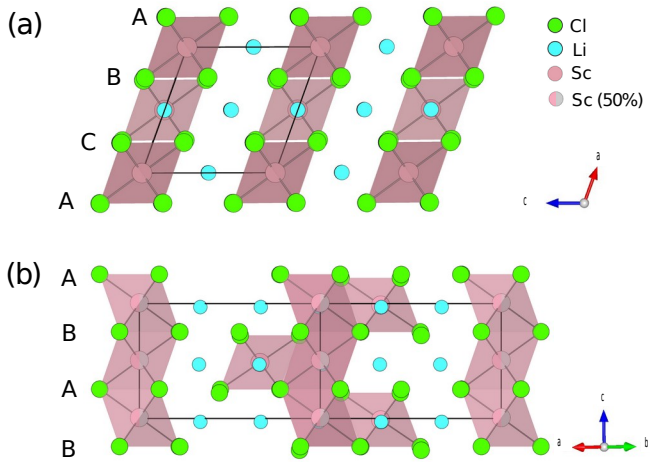

Figure 3. Structural comparison among the three different crystalline polymorphs of Li_3ScCl_6. (a) α-Li_3ScCl_6; (b) γ-Li_3ScCl_6. Inequivalent close-packed layers are labeled with the letters A, B, C, in the case of ccp, and A, B in the case of hcp. The Cl--Cl in α-Li_3ScCl_6 and γ-Li_3ScCl_6 phase has ABCABC··· stacking and ABABAB···stacking, respectively.

Numerous ternary halides with the Li_3MX_6 formula (***X***: halide anions) have been extensively explored in the quest of elevated Li^+-ion conductivity.[5–7,14] In general, the arrangement of the anion sublattice exerts a profound impact on the mobility of lithium ions.[22] The anion sublattice in Li_3MX_6 can be categorized as either ccp or hcp. Strikingly, no prior investigations have been conducted to unravel the underlying principles of solid-state chemistry that underpin the differentiation between these two classes of anion sublattice. The acquisition of γ-Li_3ScCl_6 in this study allows, for the first time, a comparison between ~~the~~ polymorphs (γ-phase and α-phase) of identical composition, thus permitting a comprehensive ~~comparison~~ analysis of ~~to determine~~ the factors governing the anion sublattice.

The alternation of anion sublattice induced by external pressure is not readily understood because not only the ccp-to-hcp conversion, as seen in In_2O_3 (from bixbyite to corundum)[34] but also the hcp-to-ccp conversion, as seen in Fe_2SiO_4 (from olivine to spinel),[35] have been reported. Consequently, we examined the relationship between the ionic radius ratio of M^{3+} to X^-, denoted as r_M/r_X, and the coordination geometry surrounding M^{3+} within the ternary Li-***M***-***X*** system ~~(X: halogen)~~, including Li_3MX_6 and $LiMF_4$, all obtained at ambient pressure. Figure 4 summarizes our findings. In accordance with Pauling's first rule, $LiMF_4$ with $r_M/r_X > 0.592$ has an MF_8 square antiprism coordination,[14,36–38] while $LiGaCl_4$ with $r_M/r_{Cl} = 0.342$ (< 0.414) has an MCl_4 tetrahedral coordination.[39] For all the reported Li_3MX_6 compounds, the r_M/r_X values fall within $0.414 < r_M/r_X < 0.592$, as expected for octahedral coordination. Surprisingly, there is a critical threshold of $(r_M/r_X)_c = 0.475$~~, i.e.,~~ ~~below~~ Below $(r_M/r_X)_c$, compounds consisting of the ccp anion-sublattice are observed, while above $(r_M/r_X)_c$, compounds consisting of the hcp anion-sublattice are observed.

This distinction, established for Li-***M***-***X*** compounds prepared under ambient pressure, cogently rationalizes the emergence of γ-Li_3ScCl_6 with hcp anion sublattice upon application of pressure. This can be interpreted by the fact that anions are more compressible than cations, so the r_{Sc}/r_{Cl} ratio increases as the radius r_{Cl} decreases more rapidly than r_{Sc} under pressure. Since $r_Y > r_{Sc}$,, the r_Y/r_{Cl} ratio already exceeds $(r_M/r_X)_c$, causing Li_3YCl_6 to take the hcp anion lattice at ambient pressure, while the γ-Li_3ScCl_6 is expected to exceed this threshold at 5 GPa of synthesis pressure. This is consistent with the empirical rule that under high pressure, elements or ions exhibit similarities to their heavier counterparts in the same group under ambient pressure.[40–42] Similarly, the high-pressure phase $LiScF_4$[36] shares its structure form with $LiYF_4$[38] and even much heavier lanthanide fluoride analog $LiLuF_4$,[43] with capped octahedral coordination.

From the standpoint of electrostatic interactions, the hcp sequence (ABAB...) with a shorter anion--anion distances between the second neighboring layers is less favorable than the ccp sequence (ABCABC...). Since the application of high pressure shortens the anion--anion distance, the conversion to the hcp sequence at high pressure in this study suggests conversely that the γ-phase of Li_3ScCl_6 is covalently stabilized. Our recent study on lanthanide hydride chalcogenides also found that there is an apparent covalent stabilization in the high-pressure phases of ***Ln***HS (***Ln*** = La, Nd, Gd, and Er) with $ChLn_6$ prismatic coordination compared to octahedral (anti-prismatic) coordination, which was supported by integrated crystal orbital Hamilton population (ICOHP) calculations.[44]

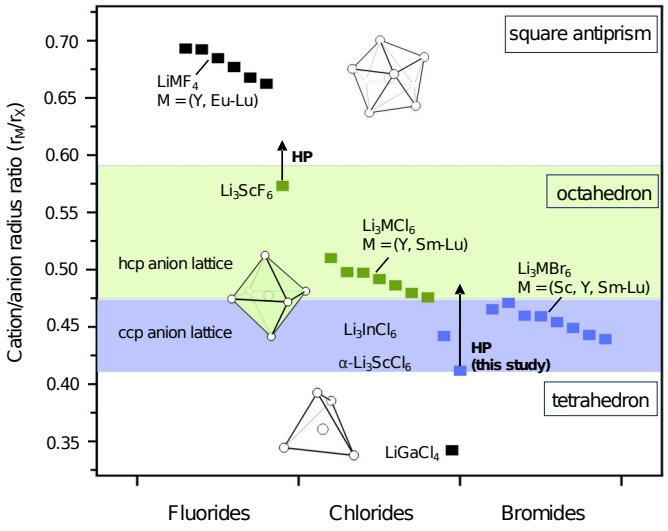

Figure 4. Relationship between the coordination environment of ***M***(III) cations and the ionic radius ratio r_M/r_X in the known Li-***M***-***X*** compounds (***X***: halogen).[14,36–39] revealing the ccp-to-hcp conversion at $r_M/r_X = 0.475$, along

with the increased coordination number (4, 6, and 8) with increasing r_M/r_X as expected from the Pauling radius rule. This picture supports the α-to-γ conversion in Li_3ScCl_6 under high pressure, along with the result of Li_3ScF_6.[36]

The switching of anion sublattices is validated by DFT calculations, comparing enthalpies of formation as a function of pressure for both the γ-Li_3ScCl_6 and α-Li_3ScCl_6 phases; note that in the γ phase, a 2×1×2 supercell with ordered lithium and Sc vacancies is constructed (see SI for details). As shown in Figure 5a, the γ phase stabilizes over the α phase above a critical pressure of about 3.7 GPa. The effective radius ratio r_{Sc}/r_{Cl} was also calculated based on the Bader charge analysis (see Figure 5c), and as anticipated, Figure 5c indicates a similar increase in r_{Sc}/r_{Cl} with pressure for both phases. This trend is consistent ~~well~~ with observations presented in Figure 4. It is important to note, however, that our discussion here remains qualitative, e.g., the calculated Sc^{3+}, Li^+, and Cl^- radii at ambient pressure are 1.33 Å, 0.95 Å, and 1.90 Å, respectively, while the Shannon radii (coordination number 6) are 0.745 Å, 0.76 Å, and 1.81 Å, respectively.

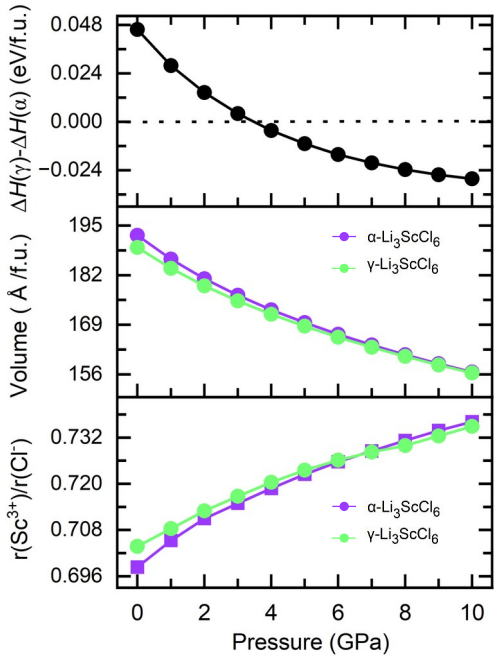

Figure 5. (top) Pressure dependence of the formation Enthalpy of γ-Li_3ScCl_6 relative to that of α-Li_3ScCl_6, demonstrating the structural transformation at about 3.7 GPa, consistent with the experimental observation. (middle) the calculated formula volume and (bottom) the effective radius ratio r_{Sc}/r_{Cl} (based on the DFT calculations) for α-Li_3ScCl_6 and γ-Li_3ScCl_6, exhibiting similar pressure dependence. Solid lines in all figures only serve as visual guides.

The investigation of the relationship between the solid electrolyte properties of Li_3MX_6 and its underlying crystal frameworks becomes possible by the acquisition of a polymorph featuring distinct anion sublattices in both ccp and hcp arrangements. Figure S6 displays the electrochemical impedance spectroscopy and temperature dependence of the ionic conductivity of γ-Li_3ScCl_6. At room temperature, the Li^+ conductivity in γ-Li_3ScCl_6 attains a value of 0.21 mS/cm, with an activation energy of 0.406 eV. ~~Remarkably, t~~The Li^+ conductivity surpasses that observed in α-Li_3YCl_6 (0.14 mS/cm)[45] and β-Li_3YCl_6 (0.12 mS/cm),[25] albeit being inferior to that of α-Li_3ScCl_6 (3.02 mS/cm) having two- and three-dimensional pathways (Figures S7 and S8).[6] We employed the bond valence pathway analyzer (BVPA)[46] to access the lithium migration energies of the structurally related materials possessing an hcp anionic lattice. The resulting migration energies are 0.73(7) eV, 0.66(4) eV, and 0.59(8) eV, respectively, for γ-Li_3ScCl_6, α-Li_3YCl_6, and β-Li_3YCl_6[25], which are larger than 0.45(2) eV for α-Li_3ScCl_6(see Figure S7). These findings align with the primary Li^+ pathways of 1D in contrast to 3D for the hcp and ccp anion lattice, respectively.[13]

Even though α-Li_3ScCl_6 was reported as the first halide SSE that could be cycled directly against Li-metal, it revealed high polarization voltage that ~~was~~ is still an issue to be resolved.[6] Cyclic voltammetry (CV)

experiments were conducted on all-solid-state Li/$Li_7P_3S_{11}$/γ-Li_3ScCl_6/γ-Li_3ScCl_6-C cells at a scan~~ning~~ rate of 0.1 mV/s to evaluate the electrochemical stability window. γ-Li_3ScCl_6 was mixed with 50 wt% carbon to improve electron conduction. For comparative analysis, the electrochemical behavior of α-Li_3ScCl_6 was also investigated. Reduction reactions in γ-Li_3ScCl_6 appear to be more subdued compared to α-Li_3ScCl_6. This is evidenced by the notably lower maximum reduction current of around 0.02 mA/cm^2, which is ~~significantly~~ an order of magnitude less than the 0.21 mA/cm^2 observed for α-Li_3ScCl_6 (see Figure S9). To further evaluate the anodic stability, symmetric cells using α- and γ-Li_3ScCl_6 were assembled, employing a Li-In alloy as the counter electrode. Charge/discharge performance~~s~~ of α- and γ-Li_3ScCl_6 over 60 min~~s~~ cycles for 1500 h are shown in Figure 6a. Notably, the Li-In/γ-Li_3ScCl_6/Li-In cell exhibited a steadier and smaller overpotential of approximately 0.32 V, in contrast to the ccp-based counterpart α-Li_3ScCl_6, which displayed an overpotential of about 1.54 V ~~for over 1500 h~~. Given that sulfide electrolytes were necessary as an additional interlayer for most Li-***M***-Cl chloride SSEs ~~between~~ against Li~~the Li anode~~,[7,8,20] these results provide compelling evidence for the improved electrochemical stability of γ-Li_3ScCl_6 toward the Li-metal anode.

Electrolytes with higher energy levels of the lowest unoccupied molecular orbital (LUMO) tend to exhibit greater resistance to electron acquisition and inherent reduction stability.[18,47] Photoelectron yield spectroscopy (PYS) (Figures S10-S11) and UV-Vis diffuse reflectance spectroscopy (Figures S12-S13) results show that the LUMO position of –2.33 eV for γ-Li_3ScCl_6 is smaller than that of –2.02 eV for α-Li_3ScCl_6 (Figure S14). These values indicate that both α-Li_3ScCl_6 and γ-Li_3ScCl_6 are not thermodynamically stable against Li-metal, and are readily reduced at low voltages. Thus the reason that α-Li_3ScCl_6 and γ-Li_3ScCl_6 can be cycled directly against Li metal can be attributed to the reduction products, such as LiCl and binary scandium subchlorides (e.g., Sc_5Cl_8 and Sc_7Cl_{10}),[6,19] forming an interphase between the electrode and electrolyte to inhibit continuous reduction reaction into the bulk electrolyte. The enhanced electrochemical stability of γ-Li_3ScCl_6 could stem from the covalent nature of the bond between Sc-t_{2g} and Cl-3*p* orbitals, as mentioned above. This covalent bond, being relatively robust, necessitates greater energy to dissociate during the reduction process, potentially favoring distinct reduction pathways. It is also possible that the high-pressure synthesis may have yielded ~~superior~~ advantageous grain boundaries and ~~particle~~ crystallite facets. Further investigation of these possibilities is a subject of future study.

Furthermore, in order to investigate the compatibility with commercialized oxide cathode, ASSBs using uncoated $LiNi_{1/3}Co_{1/3}Mn_{1/3}O_2$ (NCM111) as the cathode and Li-In as the anode without a sulfide protection layer were fabricated to examine the electrochemical performance of γ-Li_3ScCl_6 as an SSE ~~and the compatibility with NCM111~~. ASSLBs exhibit a discharge capacity of 116.2 mAh/g for the first cycle at 0.02C between 1.9 V and 3.7 V versus Li^+/Li-In. The corresponding charge-discharge curves at different C rates (including 0.02C, 0.05C, 0.1C, 0.2C, 0.5C, and 1C) are shown in Figure 6b. After the 1C-rate charge/discharge, the cell was further measured with a constant 0.1C rate during extended cycling. Li-In/γ-Li_3ScCl_6/NCM111 exhibited stable cycling and slow capacity fading from 83.8 to 74.5 mAh/g over 50 cycles between 1.9 V and 3.7 V (versus Li^+/Li-In) (see Figure 6c). The cycling stability indicates γ-Li_3ScCl_6 is a promising stable electrolyte against oxide cathode materials and the lithium metal anode.

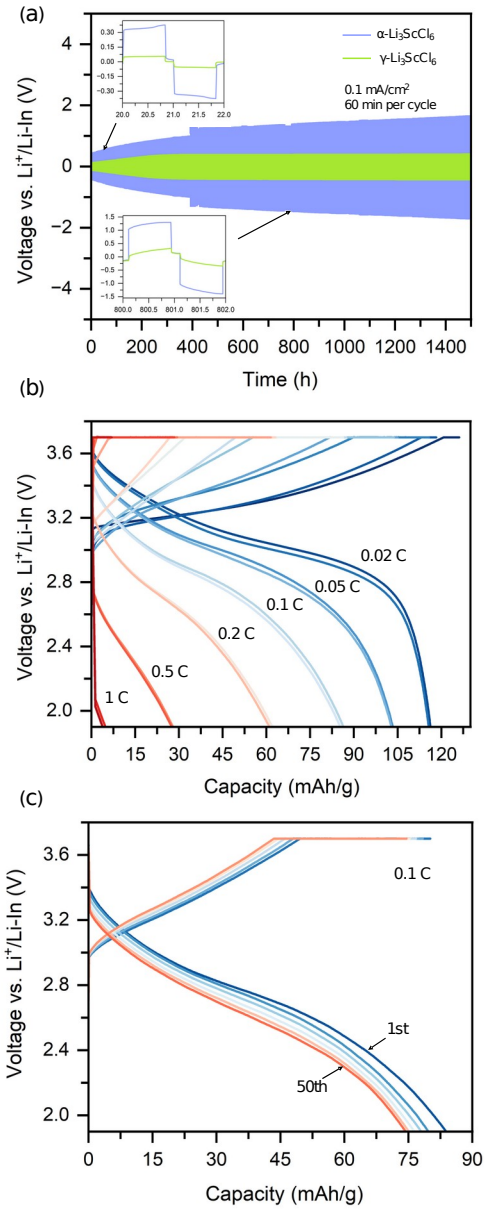

Figure 6. (a) Electrochemical performance of the symmetric all-solid-state cell, Li-In/γ-Li_3ScCl_6/Li-In, and Li-In/α-Li_3ScCl_6/Li-In respectively, at 0.1 mA/cm^{-2} (60 min per plating/stripping cycle). (b) C-rate dependence of the all-solid-state NCM111/γ-Li_3ScCl_6/In-Li cell. (c) the long-term cycling of NCM111/γ-Li_3ScCl_6/In-Li cell with 0.1C rate, showing the 1st, 11th, 21st, 31st, 41st and 50th cycles in sequence.

Conclusion

In summary, a new polymorph of Li_3ScCl_6, namely γ-Li_3ScCl_6, was obtained by high-pressure synthesis. The structure of the γ-phase was elucidated by combining single-crystal and powder X-ray diffraction and solid-state ^{7}Li and ^{45}Sc NMR spectroscopy. γ-Li_3ScCl_6 crystallizes into a hexagonal polar and chiral space group, *P*6$_3$*mc*. The ambient-pressure phases, α- and β-Li_3ScCl_6, feature a ccp anion lattice, while there is a transition to the hcp anion lattice for γ-Li_3ScCl_6, which is attributed to the increasing cation–anion radius ratio under pressure by crystal structure comparative analysis and DFT methods. The room-temperature ionic conductivity of γ-Li_3ScCl_6 is 0.21 mS/cm. Symmetric cells and Li-In/γ-Li_3ScCl_6/NCM111 all-solid-state lithium batteries show enhanced electrochemical stability of γ-Li_3ScCl_6 against the Li-In anode and stability against oxide cathodes. The results indicate that γ-Li_3ScCl_6 is a promising solid electrolyte. It could be compatible with the Li-In anode and commercialized NCM111 cathode without needing a sulfide electrolyte intermediate layer against the anode or extra coatings on the cathode.

CONFLICTS OF INTEREST

The authors declare no competing financial interest.

SUPPORTING INFORMATION

Additional synchrotron diffraction patterns at different temperatures; additional NMR data; calculated critical pressure; PYS and UV-Vis spectra; calculated density of states.
CCDC 2253017 contains the supplementary crystallographic data for this paper. These data can be obtained free of charge via www.ccdc.cam.ac.uk/data_request/cif, or by emailing data_request@ccdc.cam.ac.uk, or by contacting The Cambridge Crystallographic Data Centre, 12 Union Road, Cambridge CB2 1EZ, UK; fax: +44 1223 336033.

Acknowledgments

This work was supported by funding from **.

AUTHOR INFORMATION

Corresponding Authors

* Email: kage@scl.kyoto-u.ac.jp

REFERENCES

(1) Goodenough, J. B.; Kim, Y. Challenges for Rechargeable Li Batteries. *Chem. Mater.* **2010**, *22* (3), 587–603. https://doi.org/10.1021/cm901452z.

(2) Manthiram, A.; Yu, X.; Wang, S. Lithium Battery Chemistries Enabled by Solid-State Electrolytes. *Nat. Rev. Mater.* **2017**, *2* (4), 1–16. https://doi.org/10.1038/natrevmats.2016.103.

(3) Kamaya, N.; Homma, K.; Yamakawa, Y.; Hirayama, M.; Kanno, R.; Yonemura, M.; Kamiyama, T.; Kato, Y.; Hama, S.; Kawamoto, K.; Mitsui, A. A Lithium Superionic Conductor. *Nat. Mater.* **2011**, *10* (9), 682–686. https://doi.org/10.1038/nmat3066.

(4) Rangasamy, E.; Liu, Z.; Gobet, M.; Pilar, K.; Sahu, G.; Zhou, W.; Wu, H.; Greenbaum, S.; Liang, C. An Iodide-Based Li7P2S8I Superionic Conductor. *J. Am. Chem. Soc.* **2015**, *137* (4), 1384–1387. https://doi.org/10.1021/ja508723m.

(5) Li, X.; Liang, J.; Luo, J.; Banis, M. N.; Wang, C.; Li, W.; Deng, S.; Yu, C.; Zhao, F.; Hu, Y.; Sham, T.-K.; Zhang, L.; Zhao, S.; Lu, S.; Huang, H.; Li, R.; Adair, K. R.; Sun, X. Air-Stable Li3InCl6 Electrolyte with High Voltage Compatibility for All-Solid-State Batteries. *Energy Environ. Sci.* **2019**, *12* (9), 2665–2671. https://doi.org/10.1039/C9EE02311A.

(6) Liang, J.; Li, X.; Wang, S.; Adair, K. R.; Li, W.; Zhao, Y.; Wang, C.; Hu, Y.; Zhang, L.; Zhao, S.; Lu, S.; Huang, H.; Li, R.; Mo, Y.; Sun, X. Site-Occupation-Tuned Superionic LixScCl3+xHalide Solid Electrolytes for All-Solid-State Batteries. *J. Am. Chem. Soc.* **2020**, *142* (15), 7012–7022. https://doi.org/10.1021/jacs.0c00134.

(7) Zhou, L.; Zuo, T.-T.; Kwok, C. Y.; Kim, S. Y.; Assoud, A.; Zhang, Q.; Janek, J.; Nazar, L. F. High Areal Capacity, Long Cycle Life 4 V Ceramic All-Solid-State Li-Ion Batteries Enabled by Chloride Solid Electrolytes. *Nat. Energy* **2022**, 1–11. https://doi.org/10.1038/s41560-021-00952-0.

(8) Zhou, L.; Yuen Kwok, C.; Shyamsunder, A.; Zhang, Q.; Wu, X.; F. Nazar, L. A New Halospinel Superionic Conductor for High-Voltage All Solid State Lithium Batteries. *Energy Environ. Sci.* **2020**, *13* (7), 2056–2063. https://doi.org/10.1039/D0EE01017K.

(9) Murugan, R.; Thangadurai, V.; Weppner, W. Fast Lithium Ion Conduction in Garnet-Type Li7La3Zr2O12. *Angew. Chem. Int. Ed.* **2007**, *46* (41), 7778–7781. https://doi.org/10.1002/anie.200701144.

(10) Thompson, T.; Yu, S.; Williams, L.; Schmidt, R. D.; Garcia-Mendez, R.; Wolfenstine, J.; Allen, J. L.; Kioupakis, E.; Siegel, D. J.; Sakamoto, J. Electrochemical Window of the Li-Ion Solid Electrolyte Li7La3Zr2O12. *ACS Energy Lett.* **2017**, *2* (2), 462–468. https://doi.org/10.1021/acsenergylett.6b00593.

(11) Richards, W. D.; Miara, L. J.; Wang, Y.; Kim, J. C.; Ceder, G. Interface Stability in Solid-State Batteries. *Chem. Mater.* **2016**, *28* (1), 266–273. https://doi.org/10.1021/acs.chemmater.5b04082.

(12) Famprikis, T.; Canepa, P.; Dawson, J. A.; Islam, M. S.; Masquelier, C. Fundamentals of Inorganic Solid-State Electrolytes for Batteries. *Nat. Mater.* **2019**, *18* (12), 1278–1291. https://doi.org/10.1038/s41563-019-0431-3.

(13) Wang, S.; Bai, Q.; Nolan, A. M.; Liu, Y.; Gong, S.; Sun, Q.; Mo, Y. Lithium Chlorides and Bromides as Promising Solid-State Chemistries for Fast Ion Conductors with Good Electrochemical Stability. *Angew. Chem. Int. Ed.* **2019**, *58* (24), 8039–8043. https://doi.org/10.1002/anie.201901938.

(14) Li, X.; Liang, J.; Yang, X.; R. Adair, K.; Wang, C.; Zhao, F.; Sun, X. Progress and Perspectives on Halide Lithium Conductors for All-Solid-State Lithium Batteries. *Energy Environ. Sci.* **2020**, *13* (5), 1429–1461. https://doi.org/10.1039/C9EE03828K.

(15) Liu, Y.; Wang, S.; Nolan, A. M.; Ling, C.; Mo, Y. Tailoring the Cation Lattice for Chloride Lithium-Ion Conductors. *Adv. Energy Mater.* **2020**, *10* (40), 2002356. https://doi.org/10.1002/aenm.202002356.

(16) Chun, G. H.; Shim, J. H.; Yu, S. Computational Investigation of the Interfacial Stability of Lithium Chloride Solid Electrolytes in All-Solid-State Lithium Batteries. *ACS Appl. Mater. Interfaces* **2022**, *14* (1), 1241–1248. https://doi.org/10.1021/acsami.1c22104.

(17) Asano, T.; Sakai, A.; Ouchi, S.; Sakaida, M.; Miyazaki, A.; Hasegawa, S. Solid Halide Electrolytes with High Lithium-Ion Conductivity for Application in 4 V Class Bulk-Type All-Solid-State Batteries. *Adv. Mater.* **2018**, *30* (44), 1803075. https://doi.org/10.1002/adma.201803075.

(18) Xu, G.; Luo, L.; Liang, J.; Zhao, S.; Yang, R.; Wang, C.; Yu, T.; Wang, L.; Xiao, W.; Wang, J.; Yu, J.; Sun, X. Origin of High Electrochemical Stability of Multi-Metal Chloride Solid Electrolytes for High Energy All-Solid-State Lithium-Ion Batteries. *Nano Energy* **2022**, *92*, 106674. https://doi.org/10.1016/j.nanoen.2021.106674.

(19) Zhu, Y.; He, X.; Mo, Y. Origin of Outstanding Stability in the Lithium Solid Electrolyte Materials: Insights from Thermodynamic Analyses Based on First-Principles Calculations. *ACS Appl. Mater. Interfaces* **2015**, *7* (42), 23685–23693. https://doi.org/10.1021/acsami.5b07517.

(20) Li, X.; Liang, J.; Kim, J. T.; Fu, J.; Duan, H.; Chen, N.; Li, R.; Zhao, S.; Wang, J.; Huang, H.; Sun, X. Highly Stable Halide-Electrolyte-Based All-Solid-State Li–Se Batteries. *Adv. Mater.* **2022**, *34* (20), 2200856. https://doi.org/10.1002/adma.202200856.
(21) Yin, Y.-C.; Yang, J.-T.; Luo, J.-D.; Lu, G.-X.; Huang, Z.; Wang, J.-P.; Li, P.; Li, F.; Wu, Y.-C.; Tian, T.; Meng, Y.-F.; Mo, H.-S.; Song, Y.-H.; Yang, J.-N.; Feng, L.-Z.; Ma, T.; Wen, W.; Gong, K.; Wang, L.-J.; Ju, H.-X.; Xiao, Y.; Li, Z.; Tao, X.; Yao, H.-B. A LaCl3-Based Lithium Superionic Conductor Compatible with Lithium Metal. *Nature* **2023**, *616* (7955), 77–83. https://doi.org/10.1038/s41586-023-05899-8.
(22) Wang, Y.; Richards, W. D.; Ong, S. P.; Miara, L. J.; Kim, J. C.; Mo, Y.; Ceder, G. Design Principles for Solid-State Lithium Superionic Conductors. *Nat. Mater.* **2015**, *14* (10), 1026–1031. https://doi.org/10.1038/nmat4369.
(23) Yamane, H.; Shibata, M.; Shimane, Y.; Junke, T.; Seino, Y.; Adams, S.; Minami, K.; Hayashi, A.; Tatsumisago, M. Crystal Structure of a Superionic Conductor, Li7P3S11. *Solid State Ion.* **2007**, *178* (15), 1163–1167. https://doi.org/10.1016/j.ssi.2007.05.020.
(24) Liang, J.; Li, X.; Adair, K. R.; Sun, X. Metal Halide Superionic Conductors for All-Solid-State Batteries. *Acc. Chem. Res.* **2021**, *54* (4), 1023–1033. https://doi.org/10.1021/acs.accounts.0c00762.
(25) Ito, H.; Shitara, K.; Wang, Y.; Fujii, K.; Yashima, M.; Goto, Y.; Moriyoshi, C.; Rosero-Navarro, N. C.; Miura, A.; Tadanaga, K. Kinetically Stabilized Cation Arrangement in Li3YCl6 Superionic Conductor during Solid-State Reaction. *Adv. Sci.* **2021**, *8* (15), 2101413. https://doi.org/10.1002/advs.202101413.
(26) Hilleke, K. P.; Bi, T.; Zurek, E. Materials under High Pressure: A Chemical Perspective. *Appl. Phys. A* **2022**, *128* (5), 441. https://doi.org/10.1007/s00339-022-05576-z.
(27) Kresse, G.; Furthmüller, J. Efficiency of Ab-Initio Total Energy Calculations for Metals and Semiconductors Using a Plane-Wave Basis Set. *Comput. Mater. Sci.* **1996**, *6* (1), 15–50. https://doi.org/10.1016/0927-0256(96)00008-0.
(28) Kresse, G.; Joubert, D. From Ultrasoft Pseudopotentials to the Projector Augmented-Wave Method. *Phys. Rev. B* **1999**, *59* (3), 1758–1775. https://doi.org/10.1103/PhysRevB.59.1758.
(29) Perdew, J. P.; Ruzsinszky, A.; Csonka, G. I.; Vydrov, O. A.; Scuseria, G. E.; Constantin, L. A.; Zhou, X.; Burke, K. Restoring the Density-Gradient Expansion for Exchange in Solids and Surfaces. *Phys. Rev. Lett.* **2008**, *100* (13), 136406. https://doi.org/10.1103/PhysRevLett.100.136406.
(30) A Consistent and Accurate Ab Initio Parametrization of Density Functional Dispersion Correction (DFT-D) for the 94 Elements H-Pu.
(31) Tang, W.; Sanville, E.; Henkelman, G. A Grid-Based Bader Analysis Algorithm without Lattice Bias. *J. Phys. Condens. Matter* **2009**, *21* (8), 084204. https://doi.org/10.1088/0953-8984/21/8/084204.
(32) Schlem, R.; Banik, A.; Ohno, S.; Suard, E.; Zeier, W. G. Insights into the Lithium Sub-Structure of Superionic Conductors Li3YCl6 and Li3YBr6. *Chem. Mater.* **2021**, *33* (1), 327–337. https://doi.org/10.1021/acs.chemmater.0c04352.
(33) Brese, N. E.; O'Keeffe, M. Bond-Valence Parameters for Solids. *Acta Crystallogr. B* **1991**, *47* (2), 192–197. https://doi.org/10.1107/S0108768190011041.
(34) *Metastability of Corundum-Type In2O3*. https://doi.org/10.1002/chem.200701830.
(35) Navrotsky, A.; Akaogi, M. The α, β, γ Phase Relations in Fe2SiO4-Mg2SiO4 and Co2SiO4-Mg2SiO4: Calculation from Thermochemical Data and Geophysical Applications. *J. Geophys. Res. Solid Earth* **1984**, *89* (B12), 10135–10140. https://doi.org/10.1029/JB089iB12p10135.
(36) Tyagi, A. K.; Köhler, J.; Balog, P.; Weber, J. Syntheses and Structures of Li3ScF6 and High Pressure LiScF4−, Luminescence Properties of LiScF4, a New Phase in the System LiF–ScF3. *J. Solid State Chem.* **2005**, *178* (9), 2620–2625. https://doi.org/10.1016/j.jssc.2005.04.038.
(37) Sorokin, N. I.; Karimov, D. N.; Komar'kova, O. N. Electrophysical Properties of LiYbF4 Crystals. *Crystallogr. Rep.* **2010**, *55* (3), 448–449. https://doi.org/10.1134/S1063774510030132.
(38) Garcia, E.; Ryan, R. R. Structure of the Laser Host Material LiYF4. *Acta Crystallogr. C* **1993**, *49* (12), 2053–2054. https://doi.org/10.1107/S0108270193005876.
(39) Hönle, W.; Hettich, B.; Simon, A. Darstellung Und Kristallstrukturen von LiGaCl4 Und LiGaI4/ Preparation and Crystal Structure of LiGaCL4 and LiGaI4. *Z. Für Naturforschung B* **1987**, *42* (2), 248–250. https://doi.org/10.1515/znb-1987-0222.
(40) Prewitt, C. T.; Downs, R. T. Chapter 9. HIGH-PRESSURE CRYSTAL CHEMISTRY. In *Ultrahigh Pressure Mineralogy*; Hemley, R. J., Ed.; De Gruyter, 1998; pp 283–318. https://doi.org/10.1515/9781501509179-011.
(41) Miao, M.; Sun, Y.; Zurek, E.; Lin, H. Chemistry under High Pressure. *Nat. Rev. Chem.* **2020**, *4* (10), 508–527. https://doi.org/10.1038/s41570-020-0213-0.
(42) Zhang, L.; Wang, Y.; Lv, J.; Ma, Y. Materials Discovery at High Pressures. *Nat. Rev. Mater.* **2017**, *2* (4), 1–16. https://doi.org/10.1038/natrevmats.2017.5.
(43) Dobretsova, E. A.; Xia, X.; Pant, A.; Lim, M. B.; De Siena, M. C.; Boldyrev, K. N.; Molchanova, A. D.; Novikova, N. N.; Klimin, S. A.; Popova, M. N.; Chen, Y.; Majumdar, A.; Gamelin, D. R.; Pauzauskie, P. J. Hydrothermal Synthesis of Yb3+: LuLiF4 Microcrystals and Laser Refrigeration of Yb3+: LuLiF4/Silicon-Nitride Composite Nanostructures. *Laser Photonics Rev.* **2021**, *15* (10), 2100019. https://doi.org/10.1002/lpor.202100019.
(44) Ubukata, H.; Kato, D.; Kitade, S.; Broux, T.; Tassel, C.; Schnieders, D.; Dronskowski, R.; Kageyama, H. Structural Transformation in LnHS (Ln = La, Nd, Gd, and Er) with Coordination Change between an S-Centered Octahedron and a Trigonal Prism. *Inorg. Chem.* **2023**, *62* (17), 6696–6703. https://doi.org/10.1021/acs.inorgchem.3c00238.
(45) Asano, T.; Sakai, A.; Ouchi, S.; Sakaida, M.; Miyazaki, A.; Hasegawa, S. Solid Halide Electrolytes with High Lithium-Ion Conductivity for Application in 4 V Class Bulk-Type All-Solid-State Batteries. *Adv. Mater.* **2018**, *30* (44), 1803075. https://doi.org/10.1002/adma.201803075.
(46) Wong, L. L.; Phuah, K. C.; Dai, R.; Chen, H.; Chew, W. S.; Adams, S. Bond Valence Pathway Analyzer—An Automatic Rapid Screening Tool for Fast Ion Conductors within SoftBV. *Chem. Mater.* **2021**, *33* (2), 625–641. https://doi.org/10.1021/acs.chemmater.0c03893.

(47) Goodenough, J. B.; Park, K.-S. The Li-Ion Rechargeable Battery: A Perspective. *J. Am. Chem. Soc.* **2013**, *135* (4), 1167–1176. https://doi.org/10.1021/ja3091438.

Insert Table of Contents artwork here